



face ghosting. To further enhance the results, we respectively incorporate eikonal and smooth regularizations to reduce geometric holes and surface noise. Our approach can generate high-fidelity 3D meshes in the single image-to-3D downstream task with approximately 1 minute, significantly outperforming previous methods.

## 1 Introduction

3D content technologies allow us to create realistic digital representations of objects, environments and characters, enabling immersive experiences in virtual reality, gaming, animation and various other fields. Some approaches such as [41, 4, 23] distill 3D geometry with priors from powerful 2D diffusion model via Score Distillation Sampling (SDS), setting a new standard for integrating generalizability into 3D generation. However, these optimization-based methods often struggle with hours-long optimization time and over-saturated generation results.

Recently, multi-view diffusion has garnered significant attention due to its superior generalizability, quality, and efficiency, which facilitates the emergence of multi-view methods. By fine-tuning original 2D diffusion models on 3D dataset [10, 9], multi-view methods first generate multi-view images of a 3D object based on an image or text prompt and then extract 3D geometry through multi-view reconstruction. Compared to SDS-based approaches, such methods can generate more consistent 3D geometric shapes without Janus problem and take only a few minutes to complete, significantly improving the efficiency of generation.

However, current multi-view diffusion models only generate sparse and inconsistent images owing to the limited computational resources. The sparse views and inconsistencies in the generated images add difficulty to reconstructing high-quality meshes. Since directly optimizing on mesh representation is challenging due to its difficult deformation operations, previous 3D generation works [30, 28, 26, 16, 20] mostly train a NeRF-based representation, such as [63, 31] to reconstruct meshes from multi-view images. However, the training process of NeRF-based representation requires extensive time and resources, especially for high-resolution outputs. Additionally, it is unable to acquire the textured mesh in an end-to-end manner and relies on extra procedures such as Marching Cubes [32] to extract the iso-surface, often resulting in meshes with grid aliasing issues.

To overcome the limitations above, our key insight is to design an end-to-end mesh reconstruction framework from multi-view images. Therefore, we propose a novel mesh reconstruction framework, coined FlexiDreamer, by using an advanced gradient-based mesh optimization method FlexiCubes. With FlexiCubes, our approach can extract an explicit mesh from a learned signed distance function for iterative rendering and optimization, able to acquire textured mesh as the final output at the end of training. Furthermore, we render the mesh by surface rendering [19], which circumvents the slow rendering procedure in NeRF-based methods and diminishes generation time.

However, directly incorporating FlexiCubes into our reconstruction framework for 3D generation task is non-trivial. Firstly, given that there exist inconsistent details in multi-view images, we incorporate a hybrid positional encoding into the learning scheme of signed distance function to improve the geometry of reconstruction results. Then, due to the inaccuracies in the overlap area of two adjacent images, we design an orientation-aware texture mapping strategy for the mesh to mitigate surface ghosting. Finally, since regularizations in FlexiCubes are limited for reconstructing high-quality results, we additionally employ eikonal regularization and two smooth regularizations to avoid geometric holes and minimize noise of mesh surface.

In summary, FlexiDreamer is an end-to-end framework based on FlexiCubes that obtains the target 3D meshes without extra procedures. Combined with image-conditioned multi-view diffusion models, FlexiDreamer enables a rapid generation of photorealistic textured meshes from single-view images in approximately 1 minute on a single NVIDIA A100 GPU.

## 2 Related Works

### 2.1 3D Generation with Diffusion Models

Recently, 2D diffusion models have achieved notable success in text-to-image generation [46]. However, extending it to 3D generation poses a significant challenge. Existing 3D native diffusion

models such as [17, 39, 14, 15, 29, 8, 1, 3, 38, 66, 82, 74] can generate consistent 3D assets within seconds, but they struggle to achieve open-vocabulary 3D generation due to the limited availability of extensive 3D training datasets. On the other hand, inspired by the remarkable progress of text-to-image synthesis in 2D diffusion models, DreamFusion [41] first proposes to distill 3D geometry and appearance from 2D diffusion priors via Score Distillation Sampling (SDS). Later methods [68, 23, 4, 21, 60, 6, 33, 44, 67, 49, 35, 62, 56, 11, 22] build on DreamFusion and further enhance the quality of generated outputs. To tackle potential issues such as the Janus problem, [54, 64, 43, 76] strengthen the semantics of different views when generating multi-view images. Recently, LRM [16, 61] proposes a transformer-based reconstruction model to predict NeRF representation from single image in 5 seconds. Following works [65, 20, 72] combine LRM with pose prediction or multi-view diffusion model to perform a rapid and diverse generation. Moreover, some approaches, such as [7, 59, 77, 83, 78, 25, 5, 45, 79, 71, 58, 57, 70, 36, 58, 69], choose Gaussian Splatting [18] or FlexiCubes [51] as an alternative 3D representation in reconstruction to avoid the costly volumetric rendering in NeRF.

## 2.2 Sparse-view Reconstruction with Multi-view Generation

The evolution of 2D lifting methods has facilitated the development of consistent multi-view image generation by diffusion models [27, 52, 73, 75, 24, 55]. With multi-view images obtained, the target 3D asset can be recovered quickly by a sparse-view reconstruction. Zero-1-to-3 [27] incorporates camera pose transformations into 2D diffusion models and realizes image-conditioned novel view synthesis. One-2-3-45 [26] trains a reconstruction framework in conjunction with Zero-1-to-3 and SparseNeuS [31], realizing a rapid 3D generation. SyncDreamer [28] uses spatial volume and depth-wise attention in a 2D diffusion model to generate multi-view consistent images. Wonder3D [30] and Zero123++ [52] extend to generate multi-view RGB and normal images with cross-domain attention layers integrated into diffusion models. These high-fidelity generated images can yield 3D reconstruction via NeuS [63] or other NeRF variants [2, 53, 13]. However, since polygonal meshes are the most widely used 3D representation in downstream tasks, an additional post-processing step, commonly achieved by Marching Cubes [32], is adopted to extract target mesh from the implicit field. This step often encounters issues such as visual artifacts, adversely affecting the quality of the final reconstructed mesh.

## 2.3 Mesh Reconstruction Method

How to reconstruct high-quality meshes from multi-view images has been a long-standing problem in Computer Vision. Classically, this is addressed by photogrammetry pipelines which integrate structure-from-motion (SfM) [47] and multi-view stereo (MVS) [48] techniques. However, these traditional mesh reconstruction methods are tailored for dense-view and real-captured input images, making them unsuitable for sparse inconsistent images generated by current multi-view diffusion models. Therefore, many previous 3D generation works [30, 28, 26, 20] obtain the final polygonal mesh by exporting NeRF representation to mesh-based representation with surface extraction such as Marching Cubes (MC) [32].

Recently, with the advancement of machine learning, many works explore gradient-based mesh reconstruction schemes, which extract surface from an implicit function encoded via convolutional networks and evaluate objectives on the mesh. DM Tet [50] utilizes a differentiable marching tetrahedra layer that converts the implicit signed distance function to explicit mesh. However, vertices of extracted mesh in DM Tet are unable to move independently, leading to surface artifacts. FlexiCubes [51] integrates flexibility to the mesh-based representation by introducing extra weight parameters. Such gradient-based surface extraction methods combined with differentiable rendering enable an end-to-end sparse-view mesh reconstruction training.

# 3 Method

In this section, we present a detailed overview of FlexiDreamer (illustrated in Figure 2). Given a single input image, our model first utilizes a pre-trained multi-view diffusion model (see Sec 3.1) to generate multi-view images. Then we develop our end-to-end mesh reconstruction framework (see 3.2) to reconstruct 3D high-quality textured mesh from multi-view images. Finally, we describe the objective function to train our reconstruction framework (see Sec 3.3).

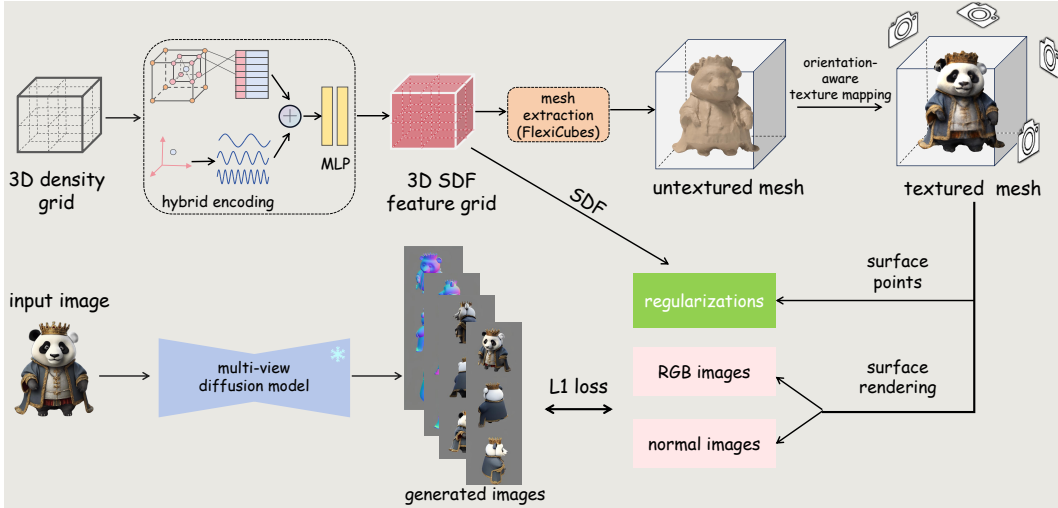


Figure 2: **The pipeline of FlexiDreamer.** The inference image is fed into multi-view diffusion model to generate multi-view images. Then an end-to-end reconstruction framework based FlexiCubes is trained end-to-end for a high-quality mesh. The mesh extracted from signed distance function can be iteratively optimized by minimizing the difference between its rendering images and multi-view generated images.

### 3.1 Multi-view Images Generation with Diffusion Model

As illustrated in Figure 2, we adopt a two-step image-to-3D pipeline. We firstly take advantage of a single image to a pre-trained multi-view diffusion model to generate multi-view RGB images. Specifically, we adopt Zero123++ [52], which is a high-performance diffusion model for multi-view images generation, to produce 6 images with evenly distributed azimuths and interleaving elevations of  $-10^\circ$  and  $20^\circ$ . Since pure RGB images supervision may bring geometry degradation (See 4.4.5 for details), we generate corresponding normal images from RGB images by a pre-trained ControlNet [80] to provide additional geometry information supervision for mesh reconstruction.

### 3.2 End-to-end Mesh Reconstruction Framework

#### 3.2.1 Architecture based on FlexiCubes

Our mesh reconstruction framework is built upon FlexiCubes [51], which directly optimizes the textured mesh by minimizing the difference with multi-view generated images. During each training iteration, we employ a neural network to estimate the signed distance function (SDF) for a pre-defined 3D density grid space. Then we use FlexiCubes to extract an untextured mesh according to the zero-level set of the signed distance function by Dual Marching Cube algorithm [40]. To obtain the texture of mesh, we query the colors of vertices from multi-view images by surface rendering [19]. The textured mesh can be iteratively optimized with the neural signed distance function network parameters through backpropagation, driven by the losses between mesh’s rendered images and multi-view generated images. With these designs, our mesh reconstruction framework supports an end-to-end training, yielding a high-quality textured mesh as the final output.

#### 3.2.2 Hybrid Positional Encoding in SDF Learning

To achieve computational efficiency during training, we adopt Instant-NGP [37] to represent signed distance function (SDF). Instant-NGP can fasten the convergence of SDF geometric fitting by utilizing a multi-scale hash encoding to encode positions into learnable features of a hash table. In this encoding scheme, a given point  $x$  is mapped to its corresponding position at each grid resolution and its feature is obtained through tri-linear interpolation. Features from all resolutions are concatenated together to form  $x$ ’s hash grid encoding features  $\gamma_h(x)$ .

However, the geometry representation based on discrete grids in Instant-NGP often leads to non-smooth and distorted reconstruction surface with the supervision of sparse and inconsistent multi-view images. To enhance reconstruction quality, we provide more geometric priors by designing a hybrid positional encoding:

We combine fourier encoding features of  $\mathbf{x}$  with its hierarchical hash grid features to mitigate the geometry distortion issue. Specifically, we firstly feed  $\mathbf{x}$  into sinusoidal functions with low frequency levels ( $m$  levels) to obtain its fourier features  $\gamma_f(\mathbf{x})$ :

$$\gamma_f(\mathbf{x}) = [\sin(\mathbf{x}), \cos(\mathbf{x}), \dots, \sin(2^{m-1}\mathbf{x}), \cos(2^{m-1}\mathbf{x})] \quad (1)$$

Then we input the concatenation of  $\gamma_h(\mathbf{x})$  and  $\gamma_f(\mathbf{x})$  into a tiny MLP characterized by shallow layers and low-dimensional hidden units. Therefore, the computational load of our neural network with this combined positional encoding remains relatively low compared to Instant-NGP and our network is still able to realize a fast convergence. Furthermore, to balance the combination of two features, we multiply hash grid features by a ratio  $\alpha$  (see Sec C.2 for details):

$$\gamma_b(\mathbf{x}) = (\gamma_f(\mathbf{x}), \alpha \cdot \gamma_h(\mathbf{x})) \quad (2)$$

to obtain the final hybrid positional encoding features  $\gamma_b(\mathbf{x})$ . Moreover, the addition of low-level fourier encoding features also helps capture more surface details, because it improves the limited representation power of the coarse-level grids of the multi-resolution hash grid encoding (see Sec 4.4.1 for details).

### 3.2.3 Orientation-aware Texture Mapping

We also adopt an orientation-aware texture mapping strategy to tolerate inconsistencies across different views of generated RGB images. Specifically, we first choose the nearest viewpoint of 6 views for each surface point on mesh by measuring the angle between their vertex normal and viewing direction. The nearest viewpoint for each surface point is determined by the smallest angle between its normal and the viewing direction. Then we assign the pixel color in the nearest-view image to each point based on its texture coordinate. This configuration helps mitigate negative effects from the inaccuracies at the overlap area of two adjacent views on the textured mesh.

### 3.2.4 Regularizations for Better Geometry

We further improve the reconstruction quality by incorporating some extra regularizations into FlexiCubes. Lacking in dense and rich-textured supervised multi-view images, we incorporate additional geometric priors to our mesh reconstruction framework by applying an eikonal regularization:

$$\mathcal{R}_{eikonal} = \frac{1}{K} \sum_{i=1}^K (\|\nabla f(\mathbf{x}_i)\| - 1)^2 \quad (3)$$

where  $K$  is the number of points in the 3D density grid while  $f$  represents the signed distance function. This design is inspired from the volumetric rendering in NeuS [63], where it is employed to constrain the magnitude of SDF gradients to be unit length. In this work, we verify its effectiveness in our surface rendering procedure of mesh (see Sec 4.4.4 for details). Moreover, since the surface of extracted mesh by FlexiCubes is rough, we adopt a laplacian regularization  $\mathcal{R}_{laplacian}$  inspired by [34]. It helps make the surface smoother by minimizing each vertex’s distance to the average position of its neighbours. We also integrate a normal consistency regularization  $\mathcal{R}_{consistency}$  to further smooth the mesh by minimizing the negative cosine similarity between connected face normals (see Sec 4.4.3 for details).

## 3.3 Training Objectives

The overall objective function of FlexiDreamer is defined as:

$$\mathcal{L}_{total} = \mathcal{L}_{rgb} + \mathcal{L}_{mask} + \mathcal{L}_{normal} + \mathcal{R}_{eikonal} + \mathcal{R}_{laplacian} + \mathcal{R}_{consistency} \quad (4)$$

where we compute a L1 loss between the rendered images and multi-view images for  $\mathcal{L}_{mask}$ ,  $\mathcal{L}_{normal}$  and  $\mathcal{L}_{rgb}$ .  $\mathcal{R}_{eikonal}$ ,  $\mathcal{R}_{laplacian}$  and  $\mathcal{R}_{consistency}$  discussed in Sec 3.2.4 are also utilized to avoid undesired reconstruction artifacts.

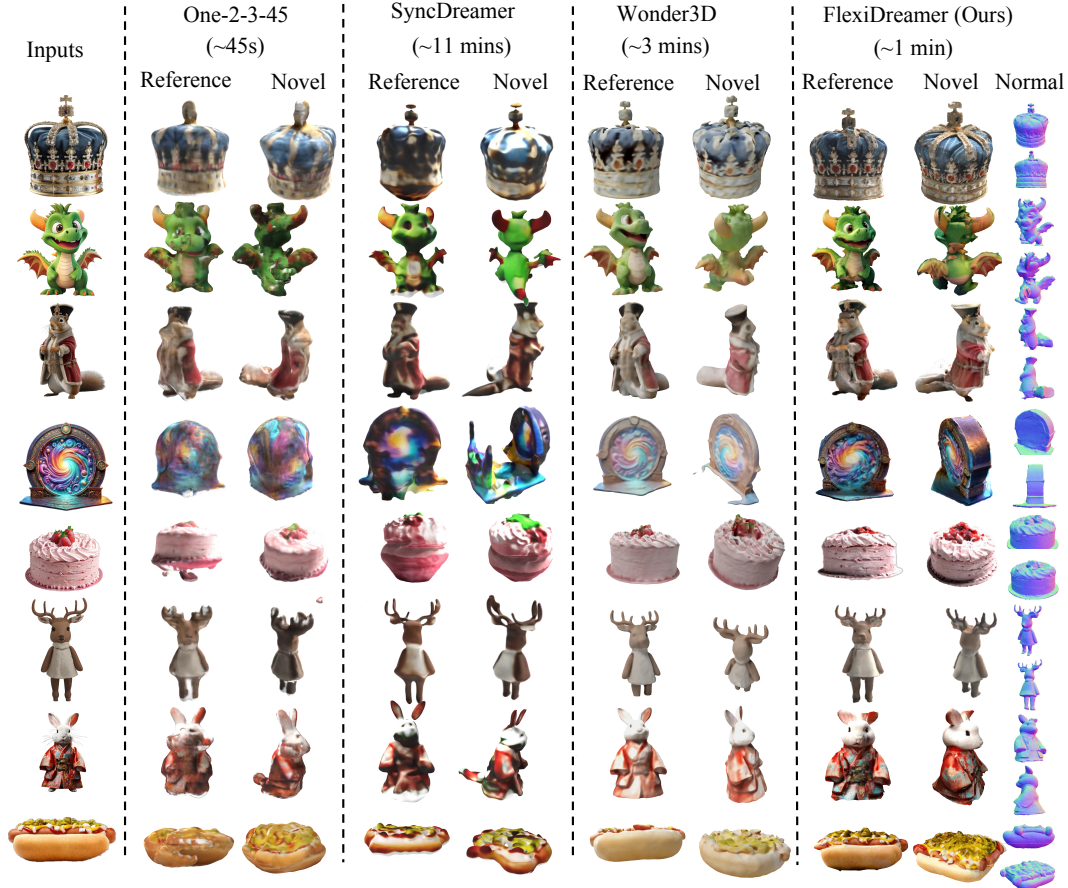


Figure 3: The qualitative comparisons with baselines in terms of the generated textured meshes. It reveals a superior performance of FlexiDreamer in reconstructing both geometry and texture details from single-view images.

## 4 Experiments

### 4.1 Implementation Details

In practice, the pre-trained multi-view diffusion model in FlexiDreamer is adopted from Zero123++[52], because it has a high performance for multi-view image generation task.

We train our reconstruction framework for 600 iterations and utilize an Adam optimizer to optimize the neural networks for signed distance function and texture with learning rates of  $1e-3$  and  $1e-2$  respectively. The network to represent signed distance function has three-layers of MLP while the network to represent texture has one layer. The geometry constraints weights, denoted as  $\lambda_{normal}$  and  $\lambda_{mask}$ , are configured to 2.0 and 15.0 respectively for geometry supervision, and  $\lambda_{rgb}$  is carefully set to 0.1 to supervise a more realistic texture. The weight assigned to the eikonal regularization, denoted as  $\lambda_{eikonal}$ , is set to 0.1. Additionally, we set  $\lambda_{laplacian}$  to 0.4 and  $\lambda_{consistency}$  to 0.05 for laplacian regularization and normal consistency regularization to obtain a smoother mesh surface. The grid resolution of 3D density grid is set to 96 to strike a balance between generation speed and quality (see Sec C.1 for details).

### 4.2 Qualitative Results

To illustrate FlexiDreamer’s scalability on single image-to-3d task, we qualitatively compare its performance with previous works. The implementation is based on their official open-source code with default parameters.

Table 1: Quantitative comparisons for geometry and texture quality between our method and baselines for single image-to-3D task on Google Scanned Object (GSO) [12] dataset.

Method	Chamfer Dist↓	Volume IoU↑	F-score (%) ↑	LPIPS↓	Clip-Sim ↑	Time
Wonder3D[30]	0.0186	0.4398	76.75	0.2554	83.70	3 min
SyncDreamer[28]	0.0140	0.3900	75.74	0.2591	82.76	11 min
One-2-3-45[26]	0.0172	0.4463	72.19	0.2625	79.83	45 s
Magic123[42]	0.0188	0.3714	60.66	0.2442	85.16	1 h
LGM [58]	0.0117	0.4685	68.69	0.2560	85.20	1 min
Ours	<b>0.0098</b>	<b>0.5078</b>	<b>78.23</b>	<b>0.2398</b>	<b>87.63</b>	1 min

Figure 3 visualizes some examples of the shapes generated from single images in geometry, texture and speed. It can be seen that compared to baselines, our method produces sharper geometric details, more distinct textures, and more consistent surfaces in a short amount of time. This is because our mesh reconstruction model based on FlexiCubes [51] optimizes the mesh by fast surface rendering and integrates more priors to reconstruct geometry from multi-view generated images. Additionally, our method also enables an end-to-end training with textured mesh as the final output, thus bypassing slow post-extraction adopted in baselines.

In Appendix, we show more comparisons with baselines and more results of high-fidelity textured meshes generated by our method.

### 4.3 Quantitative Results

We choose Google Scanned Object (GSO) dataset [12] to evaluate our method. Firstly, we scale all the generated and ground-truth meshes to an identical size and align their centers at the same position. We also carefully adjust their poses for more accurate evaluation. Subsequently, we employ Chamfer Distances (CD), Volume IoU and F-score (with a threshold of 0.05) to assess the similarity in geometry. Results on the left side of table 1 demonstrates that our method outperforms all the baselines in reconstructing accurate geometric shapes.

Additionally, to evaluate the quality of mesh texture, we respectively render 24 images from ground-truth and generated meshes. Then we use LPIPS[81] and Clip-Similarity metrics to measure the resemblance of their appearance. Results on the right side of table 1 summarizes that our method outperforms all the baselines in recovering realistic texture.

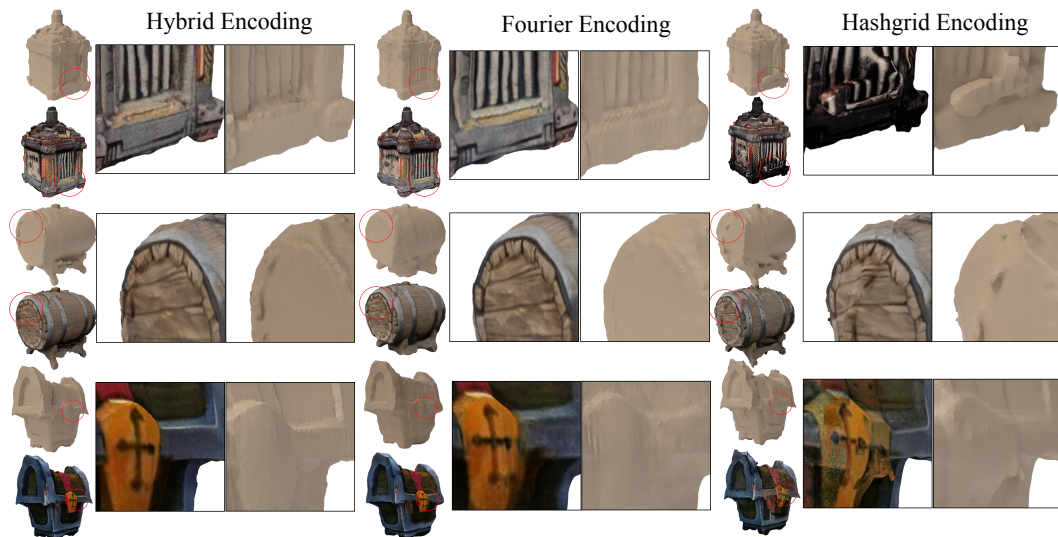


Figure 4: Results of using different encoding scheme. Compared to fourier encoding and hashgrid encoding scheme, our model with hybrid encoding generates the most accurate geometry and texture.

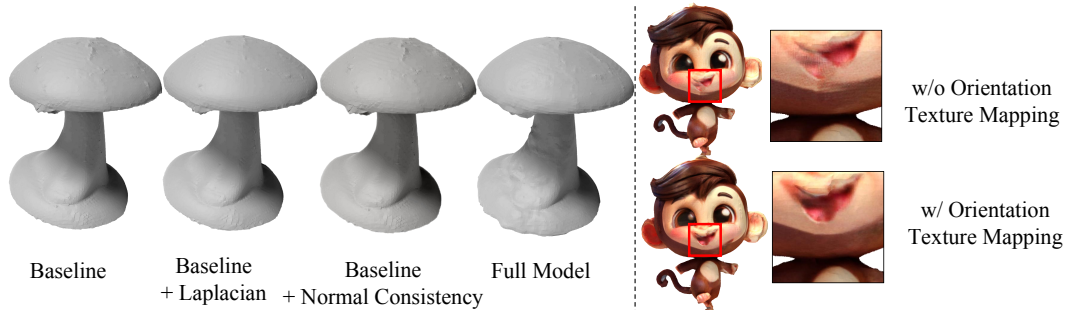


Figure 5: Ablation study on the smooth regularizations and orientation texture mapping strategy. For smooth regularization, the laplacian smoothing term can smooth the surface of the mesh at a global scale while normal consistency constraint helps reduce high-frequency noises. For orientation texture mapping, it can be seen that it is helpful for mitigating surface ghosting.

#### 4.4.1 Design of Hybrid Positional Encoding

We examine the feasibility of adopting a hybrid position encoding scheme in signed distance function (SDF) learning to reduce geometry distortions. We respectively integrate fourier positional encoding, hybrid positional encoding and multi-resolution hash grid encoding into the SDF neural network and compare the geometry of their final mesh results. In Figure 4, we can find that both fourier encoding and hash grid encoding are unable to reconstruct an accurate geometry from multi-view images, because the former generates over-smooth surface (more clearly in the second example) and the latter makes reconstruction shapes distorted. In contrast, the hybrid encoding can mitigate the geometry distortion and generate a more detailed surface.

#### 4.4.2 Orientation-aware Texture Mapping Strategy

We validate the effectiveness of our proposed orientation-aware texture mapping. To compare, we train our reconstruction framework with a trivial texture mapping. The results are illustrated in the right side of Figure 5. It can be figured out that the meshes without using orientation-aware texture mapping have severe ghosting problems on the surface, due to the inconsistent details existing in supervised RGB images. On the contrary, the meshes reconstructed with orientation-aware texture mapping strategy have a more accurate appearance. However, this strategy is unable to fully address the inconsistencies of multi-view images. We will explore to further overcome this challenge for future work.

#### 4.4.3 Smooth Regularization

To assess the effectiveness of the two smooth regularizations we employed, which are laplacian regularization and normal consistency regularization, we conduct experiments in generating a mushroom featuring a smooth cap. The visualization results are depicted in the left side of Figure 5 (please zoom in to see them more clearly). It is noticed that the baseline model’s surface exhibits severe unevenness. Incorporating either laplacian smoothness or normal consistency constraints can help mitigate the noisy surfaces. Specifically, the laplacian penalty term is adept at smoothing the mesh surface at a global scale. Meanwhile, the normal consistency term plays a pivotal role in diminishing high-frequency noises, thereby enhancing the overall quality of the mesh structure. Finally, the combination of both smoothing strategies yields optimal performance, resulting in clean surfaces while retaining intricate details.

#### 4.4.4 Eikonal Regularization

To assess the effectiveness of eikonal regularization integrated in the model, we respectively train FlexiDreamer with and without  $\mathcal{R}_{eikonal}$ . The comparison of reconstruction results are shown in Figure 6 (a). We can see that the meshes generated without eikonal constraints have geometric holes or outliers. This illustrates that eikonal regularization is helpful for our model, which is featured by surface rendering, in constraining signed distance function to represent a complete geometry.



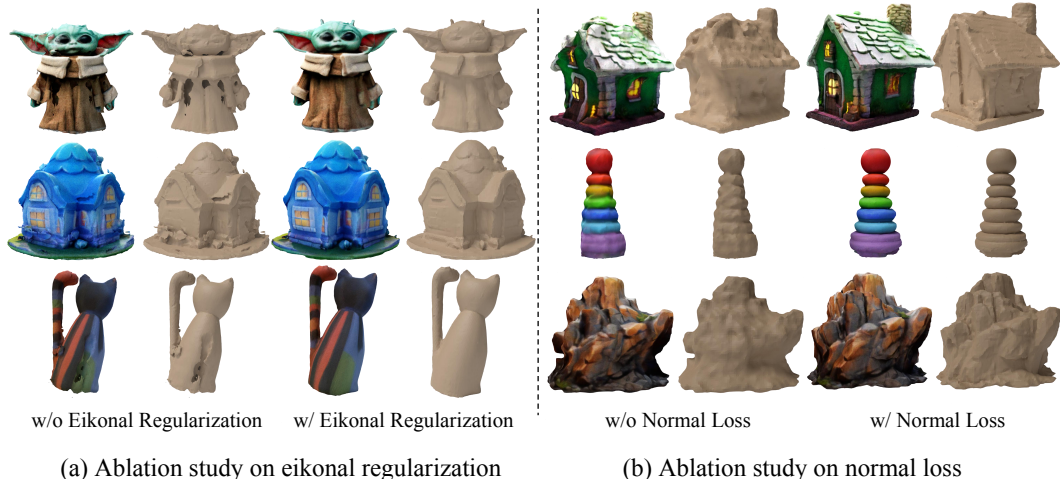


Figure 6: Ablation study on eikonal regularization and normal loss respectively. (a) Without employing eikonal regularization, the reconstruction geometry has holes or outliers. (b) Without supervision of normal images, the geometric shapes of results are not correct, and sometimes degrade.

#### 4.4.5 The Importance of Normal Loss

We examine the significance of normal images supervision to reconstruction results. To compare, we train FlexiDreamer without  $\mathcal{L}_{normal}$ . The results are shown in Figure 6 (b). It is evident that the results generated without normal constraints suffer from severe geometry degradation. This is because normal images can provide crucial geometric information for the reconstruction process, especially when dealing with complex geometric shapes.

## 5 Conclusion

In this paper, we introduce FlexiDreamer, a novel framework for generating high-quality textured meshes from single-view images. By utilizing a gradient-based mesh optimization method FlexiCubes, FlexiDreamer realizes a rapid end-to-end acquisition of target textured meshes without extra procedure like Marching Cubes. We adopt a hybrid encoding scheme and a texture mapping strategy to tolerate the inconsistencies from multi-view generated images respectively in reconstruction geometry and texture. To further enhance the reconstruction results, we integrate extra regularizations into our mesh reconstruction framework for better geometry. Overall, FlexiDreamer can generate realistic textured meshes in approximately 1 minute.

### 5.1 Limitations

Given that our model is essentially a multi-view reconstruction model, the quality of 3D generated meshes is heavily dependent on the quality of multi-view images. Due to the limited ability of current multi-view diffusion model to generate dense and consistent images, some reconstruction results of FlexiDreamer are not satisfactory. Additionally, our model also struggles to generate accurate 3D geometric shapes from input images with large elevation angles. Finally, The resolution of our density grid can only be set up to 128 due to the limited computing resources, which hinders its ability to generate more detailed surface.

### 5.2 Potential Negative Impact

Although our method excels in producing hyper-realistic 3D assets within a short amount of time, the high fidelity of our generated results might raise a concern about misuse by malicious entities. Therefore, it is necessary for developers and users to remain vigilant to prevent the occurrence of such harmful practices.

## References

- [1] Ziang Cao, Fangzhou Hong, Tong Wu, Liang Pan, and Ziwei Liu. Large-vocabulary 3d diffusion model with transformer, 2023.
- [2] Anpei Chen, Zexiang Xu, Andreas Geiger, Jingyi Yu, and Hao Su. Tensorf: Tensorial radiance fields. In *European Conference on Computer Vision*, pages 333–350. Springer, 2022.
- [3] Hansheng Chen, Jiatao Gu, Anpei Chen, Wei Tian, Zhuowen Tu, Lingjie Liu, and Hao Su. Single-stage diffusion nerf: A unified approach to 3d generation and reconstruction, 2023.
- [4] Rui Chen, Yongwei Chen, Ningxin Jiao, and Kui Jia. Fantasia3d: Disentangling geometry and appearance for high-quality text-to-3d content creation. *arXiv preprint arXiv:2303.13873*, 2023.
- [5] Yiwen Chen, Zilong Chen, Chi Zhang, Feng Wang, Xiaofeng Yang, Yikai Wang, Zhongang Cai, Lei Yang, Huaping Liu, and Guosheng Lin. Gaussianeditor: Swift and controllable 3d editing with gaussian splatting, 2023.
- [6] Yiwen Chen, Chi Zhang, Xiaofeng Yang, Zhongang Cai, Gang Yu, Lei Yang, and Guosheng Lin. It3d: Improved text-to-3d generation with explicit view synthesis, 2023.
- [7] Zilong Chen, Feng Wang, and Huaping Liu. Text-to-3d using gaussian splatting. *arXiv preprint arXiv:2309.16585*, 2023.
- [8] Gene Chou, Yuval Bahat, and Felix Heide. Diffusion-sdf: Conditional generative modeling of signed distance functions, 2023.
- [9] Matt Deitke, Ruoshi Liu, Matthew Wallingford, Huong Ngo, Oscar Michel, Aditya Kusupati, Alan Fan, Christian Laforte, Vikram Voleti, Samir Yitzhak Gadre, et al. Objaverse-xl: A universe of 10m+ 3d objects. *Advances in Neural Information Processing Systems*, 36, 2024.
- [10] Matt Deitke, Dustin Schwenk, Jordi Salvador, Luca Weihs, Oscar Michel, Eli VanderBilt, Ludwig Schmidt, Kiana Ehsani, Aniruddha Kembhavi, and Ali Farhadi. Objaverse: A universe of annotated 3d objects. In *Proceedings of the IEEE/CVF Conference on Computer Vision and Pattern Recognition*, pages 13142–13153, 2023.
- [11] Lihe Ding, Shaocong Dong, Zhanpeng Huang, Zibin Wang, Yiyuan Zhang, Kaixiong Gong, Dan Xu, and Tianfan Xue. Text-to-3d generation with bidirectional diffusion using both 2d and 3d priors, 2023.
- [12] Laura Downs, Anthony Francis, Nate Koenig, Brandon Kinman, Ryan Hickman, Krista Reymann, Thomas B. McHugh, and Vincent Vanhoucke. Google scanned objects: A high-quality dataset of 3d scanned household items, 2022.
- [13] Sara Fridovich-Keil, Giacomo Meanti, Frederik Warburg, Benjamin Recht, and Angjoo Kanazawa. K-planes: Explicit radiance fields in space, time, and appearance, 2023.
- [14] Jun Gao, Tianchang Shen, Zian Wang, Wenzheng Chen, Kangxue Yin, Daiqing Li, Or Litany, Zan Gojcic, and Sanja Fidler. Get3d: A generative model of high quality 3d textured shapes learned from images. *Advances In Neural Information Processing Systems*, 35:31841–31854, 2022.
- [15] Anchit Gupta, Wenhan Xiong, Yixin Nie, Ian Jones, and Barlas Oğuz. 3dgen: Triplane latent diffusion for textured mesh generation, 2023.
- [16] Yicong Hong, Kai Zhang, Jiuxiang Gu, Sai Bi, Yang Zhou, Difan Liu, Feng Liu, Kalyan Sunkavalli, Trung Bui, and Hao Tan. Lrm: Large reconstruction model for single image to 3d, 2023.
- [17] Heewoo Jun and Alex Nichol. Shap-e: Generating conditional 3d implicit functions. *arXiv preprint arXiv:2305.02463*, 2023.
- [18] Bernhard Kerbl, Georgios Kopanas, Thomas Leimkühler, and George Drettakis. 3d gaussian splatting for real-time radiance field rendering, 2023.

- [19] Samuli Laine, Janne Hellsten, Tero Karras, Yeongho Seol, Jaakko Lehtinen, and Timo Aila. Modular primitives for high-performance differentiable rendering. *ACM Transactions on Graphics*, 39(6), 2020.
- [20] Jiahao Li, Hao Tan, Kai Zhang, Zexiang Xu, Fujun Luan, Yinghao Xu, Yicong Hong, Kalyan Sunkavalli, Greg Shakhnarovich, and Sai Bi. Instant3d: Fast text-to-3d with sparse-view generation and large reconstruction model, 2023.
- [21] Weiyu Li, Rui Chen, Xuelin Chen, and Ping Tan. Sweetdreamer: Aligning geometric priors in 2d diffusion for consistent text-to-3d, 2023.
- [22] Yixun Liang, Xin Yang, Jiantao Lin, Haodong Li, Xiaogang Xu, and Yingcong Chen. Lucidreamer: Towards high-fidelity text-to-3d generation via interval score matching, 2023.
- [23] Chen-Hsuan Lin, Jun Gao, Luming Tang, Towaki Takikawa, Xiaohui Zeng, Xun Huang, Karsten Kreis, Sanja Fidler, Ming-Yu Liu, and Tsung-Yi Lin. Magic3d: High-resolution text-to-3d content creation. In *IEEE Conference on Computer Vision and Pattern Recognition (CVPR)*, 2023.
- [24] Yukang Lin, Haonan Han, Chaoqun Gong, Zunnan Xu, Yachao Zhang, and Xiu Li. Consistent123: One image to highly consistent 3d asset using case-aware diffusion priors, 2024.
- [25] Huan Ling, Seung Wook Kim, Antonio Torralba, Sanja Fidler, and Karsten Kreis. Align your gaussians: Text-to-4d with dynamic 3d gaussians and composed diffusion models, 2024.
- [26] Minghua Liu, Chao Xu, Haiyan Jin, Linghao Chen, Zexiang Xu, Hao Su, et al. One-2-3-45: Any single image to 3d mesh in 45 seconds without per-shape optimization. *arXiv preprint arXiv:2306.16928*, 2023.
- [27] Ruoshi Liu, Rundi Wu, Basile Van Hoorick, Pavel Tokmakov, Sergey Zakharov, and Carl Vondrick. Zero-1-to-3: Zero-shot one image to 3d object. In *Proceedings of the IEEE/CVF International Conference on Computer Vision*, pages 9298–9309, 2023.
- [28] Yuan Liu, Cheng Lin, Zijiao Zeng, Xiaoxiao Long, Lingjie Liu, Taku Komura, and Wenping Wang. Syncdreamer: Generating multiview-consistent images from a single-view image. *arXiv preprint arXiv:2309.03453*, 2023.
- [29] Zhen Liu, Yao Feng, Michael J. Black, Derek Nowrouzezahrai, Liam Paull, and Weiyang Liu. Meshdiffusion: Score-based generative 3d mesh modeling, 2023.
- [30] Xiaoxiao Long, Yuan-Chen Guo, Cheng Lin, Yuan Liu, Zhiyang Dou, Lingjie Liu, Yuexin Ma, Song-Hai Zhang, Marc Habermann, Christian Theobalt, et al. Wonder3d: Single image to 3d using cross-domain diffusion. *arXiv preprint arXiv:2310.15008*, 2023.
- [31] Xiaoxiao Long, Cheng Lin, Peng Wang, Taku Komura, and Wenping Wang. Sparseneus: Fast generalizable neural surface reconstruction from sparse views, 2022.
- [32] William E. Lorensen and Harvey E. Cline. Marching cubes: A high resolution 3d surface construction algorithm. In *Proceedings of the 14th Annual Conference on Computer Graphics and Interactive Techniques, SIGGRAPH '87*, page 163–169, New York, NY, USA, 1987. Association for Computing Machinery.
- [33] Jonathan Lorraine, Kevin Xie, Xiaohui Zeng, Chen-Hsuan Lin, Towaki Takikawa, Nicholas Sharp, Tsung-Yi Lin, Ming-Yu Liu, Sanja Fidler, and James Lucas. Att3d: Amortized text-to-3d object synthesis, 2023.
- [34] Fujun Luan, Shuang Zhao, Kavita Bala, and Zhao Dong. Unified shape and svbrdf recovery using differentiable monte carlo rendering, 2021.
- [35] Luke Melas-Kyriazi, Christian Ruppert, Iro Laina, and Andrea Vedaldi. Realfusion: 360deg reconstruction of any object from a single image, 2023.
- [36] Antoine Mercier, Ramin Nakhli, Mahesh Reddy, Rajeev Yasarla, Hong Cai, Fatih Porikli, and Guillaume Berger. Hexagen3d: Stablediffusion is just one step away from fast and diverse text-to-3d generation. *arXiv preprint arXiv:2401.07727*, 2024.

- [37] Thomas Müller, Alex Evans, Christoph Schied, and Alexander Keller. Instant neural graphics primitives with a multiresolution hash encoding. *ACM Trans. Graph.*, 41(4):102:1–102:15, July 2022.
- [38] Norman Müller, Yawar Siddiqui, Lorenzo Porzi, Samuel Rota Bulò, Peter Kotschieder, and Matthias Nießner. Diffirf: Rendering-guided 3d radiance field diffusion, 2023.
- [39] Alex Nichol, Heewoo Jun, Prafulla Dhariwal, Pamela Mishkin, and Mark Chen. Point-e: A system for generating 3d point clouds from complex prompts, 2022.
- [40] Gregory M Nielson. Dual marching cubes. In *IEEE visualization 2004*, pages 489–496. IEEE, 2004.
- [41] Ben Poole, Ajay Jain, Jonathan T. Barron, and Ben Mildenhall. Dreamfusion: Text-to-3d using 2d diffusion. *arXiv*, 2022.
- [42] Guocheng Qian, Jinjie Mai, Abdullah Hamdi, Jian Ren, Aliaksandr Siarohin, Bing Li, Hsin-Ying Lee, Ivan Skorokhodov, Peter Wonka, Sergey Tulyakov, and Bernard Ghanem. Magic123: One image to high-quality 3d object generation using both 2d and 3d diffusion priors, 2023.
- [43] Lingteng Qiu, Guanying Chen, Xiaodong Gu, Qi Zuo, Mutian Xu, Yushuang Wu, Weihao Yuan, Zilong Dong, Liefeng Bo, and Xiaoguang Han. Richdreamer: A generalizable normal-depth diffusion model for detail richness in text-to-3d. *arXiv preprint arXiv:2311.16918*, 2023.
- [44] Amit Raj, Srinivas Kaza, Ben Poole, Michael Niemeyer, Nataniel Ruiz, Ben Mildenhall, Shiran Zada, Kfir Aberman, Michael Rubinstein, Jonathan Barron, Yuanzhen Li, and Varun Jampani. Dreambooth3d: Subject-driven text-to-3d generation, 2023.
- [45] Jiawei Ren, Liang Pan, Jiaxiang Tang, Chi Zhang, Ang Cao, Gang Zeng, and Ziwei Liu. Dreamgaussian4d: Generative 4d gaussian splatting, 2023.
- [46] Robin Rombach, Andreas Blattmann, Dominik Lorenz, Patrick Esser, and Björn Ommer. High-resolution image synthesis with latent diffusion models. In *Proceedings of the IEEE/CVF conference on computer vision and pattern recognition*, pages 10684–10695, 2022.
- [47] Johannes L Schonberger and Jan-Michael Frahm. Structure-from-motion revisited. In *Proceedings of the IEEE conference on computer vision and pattern recognition*, pages 4104–4113, 2016.
- [48] Johannes L Schönberger, Enliang Zheng, Jan-Michael Frahm, and Marc Pollefeys. Pixelwise view selection for unstructured multi-view stereo. In *Computer Vision—ECCV 2016: 14th European Conference, Amsterdam, The Netherlands, October 11–14, 2016, Proceedings, Part III 14*, pages 501–518. Springer, 2016.
- [49] Junyoung Seo, Wooseok Jang, Min-Seop Kwak, Hyeonsu Kim, Jaehoon Ko, Junho Kim, Jin-Hwa Kim, Jiyoung Lee, and Seungryong Kim. Let 2d diffusion model know 3d-consistency for robust text-to-3d generation, 2024.
- [50] Tianchang Shen, Jun Gao, Kangxue Yin, Ming-Yu Liu, and Sanja Fidler. Deep marching tetrahedra: a hybrid representation for high-resolution 3d shape synthesis, 2021.
- [51] Tianchang Shen, Jacob Munkberg, Jon Hasselgren, Kangxue Yin, Zian Wang, Wenzheng Chen, Zan Gojcic, Sanja Fidler, Nicholas Sharp, and Jun Gao. Flexible isosurface extraction for gradient-based mesh optimization. *ACM Trans. Graph.*, 42(4), jul 2023.
- [52] Ruoxi Shi, Hansheng Chen, Zhuoyang Zhang, Minghua Liu, Chao Xu, Xinyue Wei, Linghao Chen, Chong Zeng, and Hao Su. Zero123++: a single image to consistent multi-view diffusion base model, 2023.
- [53] Ruoxi Shi, Xinyue Wei, Cheng Wang, and Hao Su. Zerorf: Fast sparse view 360deg reconstruction with zero pretraining, 2023.
- [54] Yichun Shi, Peng Wang, Jianglong Ye, Mai Long, Kejie Li, and Xiao Yang. Mvdream: Multi-view diffusion for 3d generation, 2023.

- [55] Yukai Shi, Jianan Wang, He Cao, Boshi Tang, Xianbiao Qi, Tianyu Yang, Yukun Huang, Shilong Liu, Lei Zhang, and Heung-Yeung Shum. Toss:high-quality text-guided novel view synthesis from a single image, 2023.
- [56] Jingxiang Sun, Bo Zhang, Ruizhi Shao, Lizhen Wang, Wen Liu, Zhenda Xie, and Yebin Liu. Dreamcraft3d: Hierarchical 3d generation with bootstrapped diffusion prior, 2023.
- [57] Stanislaw Szymanowicz, Christian Rupprecht, and Andrea Vedaldi. Splatter image: Ultra-fast single-view 3d reconstruction, 2023.
- [58] Jiaxiang Tang, Zhaoxi Chen, Xiaokang Chen, Tengfei Wang, Gang Zeng, and Ziwei Liu. Lgm: Large multi-view gaussian model for high-resolution 3d content creation. *arXiv preprint arXiv:2402.05054*, 2024.
- [59] Jiaxiang Tang, Jiawei Ren, Hang Zhou, Ziwei Liu, and Gang Zeng. Dreamgaussian: Generative gaussian splatting for efficient 3d content creation, 2023.
- [60] Junshu Tang, Tengfei Wang, Bo Zhang, Ting Zhang, Ran Yi, Lizhuang Ma, and Dong Chen. Make-it-3d: High-fidelity 3d creation from a single image with diffusion prior, 2023.
- [61] Dmitry Tochilkin, David Pankratz, Zexiang Liu, Zixuan Huang, Adam Letts, Yangguang Li, Ding Liang, Christian Laforte, Varun Jampani, and Yan-Pei Cao. Tripotr: Fast 3d object reconstruction from a single image, 2024.
- [62] Haochen Wang, Xiaodan Du, Jiahao Li, Raymond A. Yeh, and Greg Shakhnarovich. Score jacobian chaining: Lifting pretrained 2d diffusion models for 3d generation, 2022.
- [63] Peng Wang, Lingjie Liu, Yuan Liu, Christian Theobalt, Taku Komura, and Wenping Wang. Neus: Learning neural implicit surfaces by volume rendering for multi-view reconstruction, 2023.
- [64] Peng Wang and Yichun Shi. Imagedream: Image-prompt multi-view diffusion for 3d generation, 2023.
- [65] Peng Wang, Hao Tan, Sai Bi, Yinghao Xu, Fujun Luan, Kalyan Sunkavalli, Wenping Wang, Zexiang Xu, and Kai Zhang. Pflrm: Pose-free large reconstruction model for joint pose and shape prediction, 2023.
- [66] Tengfei Wang, Bo Zhang, Ting Zhang, Shuyang Gu, Jianmin Bao, Tadas Baltrusaitis, Jingjing Shen, Dong Chen, Fang Wen, Qifeng Chen, and Baining Guo. Rodin: A generative model for sculpting 3d digital avatars using diffusion, 2022.
- [67] Xinzhou Wang, Yikai Wang, Junliang Ye, Zhengyi Wang, Fuchun Sun, Pengkun Liu, Ling Wang, Kai Sun, Xintong Wang, and Bin He. Animatabledreamer: Text-guided non-rigid 3d model generation and reconstruction with canonical score distillation. *arXiv preprint arXiv:2312.03795*, 2023.
- [68] Zhengyi Wang, Cheng Lu, Yikai Wang, Fan Bao, Chongxuan Li, Hang Su, and Jun Zhu. Prolificdreamer: High-fidelity and diverse text-to-3d generation with variational score distillation. In *Advances in Neural Information Processing Systems (NeurIPS)*, 2023.
- [69] Zhengyi Wang, Yikai Wang, Yifei Chen, Chendong Xiang, Shuo Chen, Dajiang Yu, Chongxuan Li, Hang Su, and Jun Zhu. Crm: Single image to 3d textured mesh with convolutional reconstruction model. *arXiv preprint arXiv:2403.05034*, 2024.
- [70] Dejia Xu, Ye Yuan, Morteza Mardani, Sifei Liu, Jiaming Song, Zhangyang Wang, and Arash Vahdat. Agg: Amortized generative 3d gaussians for single image to 3d, 2024.
- [71] Yinghao Xu, Zifan Shi, Wang Yifan, Hansheng Chen, Ceyuan Yang, Sida Peng, Yujun Shen, and Gordon Wetzstein. Grm: Large gaussian reconstruction model for efficient 3d reconstruction and generation, 2024.
- [72] Yinghao Xu, Hao Tan, Fujun Luan, Sai Bi, Peng Wang, Jiahao Li, Zifan Shi, Kalyan Sunkavalli, Gordon Wetzstein, Zexiang Xu, and Kai Zhang. Dmv3d: Denoising multi-view diffusion using 3d large reconstruction model, 2023.

- [73] Jiayu Yang, Ziang Cheng, Yunfei Duan, Pan Ji, and Hongdong Li. Consistnet: Enforcing 3d consistency for multi-view images diffusion, 2023.
- [74] Lior Yariv, Omri Puny, Natalia Neverova, Oran Gafni, and Yaron Lipman. Mosaic-sdf for 3d generative models, 2023.
- [75] Jianglong Ye, Peng Wang, Kejie Li, Yichun Shi, and Heng Wang. Consistent-1-to-3: Consistent image to 3d view synthesis via geometry-aware diffusion models, 2023.
- [76] Junliang Ye, Fangfu Liu, Qixiu Li, Zhengyi Wang, Yikai Wang, Xinzhou Wang, Yueqi Duan, and Jun Zhu. Dreamreward: Text-to-3d generation with human preference, 2024.
- [77] Taoran Yi, Jiemin Fang, Junjie Wang, Guanjun Wu, Lingxi Xie, Xiaopeng Zhang, Wenyu Liu, Qi Tian, and Xinggang Wang. Gaussiandreamer: Fast generation from text to 3d gaussians by bridging 2d and 3d diffusion models, 2023.
- [78] Yuyang Yin, Dejie Xu, Zhangyang Wang, Yao Zhao, and Yunchao Wei. 4dgen: Grounded 4d content generation with spatial-temporal consistency, 2024.
- [79] Junwu Zhang, Zhenyu Tang, Yatian Pang, Xinhua Cheng, Peng Jin, Yida Wei, Munan Ning, and Li Yuan. Repaint123: Fast and high-quality one image to 3d generation with progressive controllable 2d repainting, 2023.
- [80] Lvmin Zhang, Anyi Rao, and Maneesh Agrawala. Adding conditional control to text-to-image diffusion models, 2023.
- [81] Richard Zhang, Phillip Isola, Alexei A Efros, Eli Shechtman, and Oliver Wang. The unreasonable effectiveness of deep features as a perceptual metric. In *Proceedings of the IEEE conference on computer vision and pattern recognition*, pages 586–595, 2018.
- [82] Zibo Zhao, Wen Liu, Xin Chen, Xianfang Zeng, Rui Wang, Pei Cheng, Bin Fu, Tao Chen, Gang Yu, and Shenghua Gao. Michelangelo: Conditional 3d shape generation based on shape-image-text aligned latent representation, 2023.
- [83] Zi-Xin Zou, Zhipeng Yu, Yuan-Chen Guo, Yangguang Li, Ding Liang, Yan-Pei Cao, and Song-Hai Zhang. Triplane meets gaussian splatting: Fast and generalizable single-view 3d reconstruction with transformers, 2023.

## A More Implementation Details

For multi-view image generation, we adopt Zero123++ [52] as our multi-view diffusion model. The guidance of Zero123++ is configured to 4 while the number of inference steps is set to 75. We also utilize the ControlNet integrated in Zero123++ to generate normal images from its multi-view RGB outputs.

In our hybrid encoding scheme, the level of fourier encoding  $m$  is 6 and the resolution of hierarchical hash grids is chosen to be a geometric progression between the coarsest and finest resolutions  $[2^4, 2^{10}]$  with 12 levels. Each hash entry has a channel of 2. The combination ratio of hash grid features  $\alpha$  equals to 0.1.

Our implementation is built on the official code of Zero123++ and FlexiCubes[51]. For Sec 4.2 and 4.3, we compare FlexiDreamer with several competitive baselines by using their official code on GitHub, including One-2-3-45[26], SyncDreamer[28], Wonder3D[30] Magic123[42] and LGM[58].

## B Camera Settings

We inherit the camera settings from Zero123++: In order to circumvent the error in the elevation estimation module incorporated in previous pipelines, such as One-2-3-45 [26] and DreamGaussian [59], we use camera poses with relative azimuth and absolute elevation angles to the input view for novel view synthesis to minimize the orientation inconsistency. To be more specific, the six poses comprise interleaving elevations of  $-10^\circ$  and  $20^\circ$ , accompanied by azimuths that span from  $30^\circ$  to  $330^\circ$  with an increase by  $60^\circ$  for each pose. These carefully chosen camera poses can totally scan the whole object. Moreover, we adopt a perspective camera system and the camera is positioned at a distance of 3.0 meters from the coordinate origin, i.e. the radial distance is 3.0.

## C Additional Ablation Studies

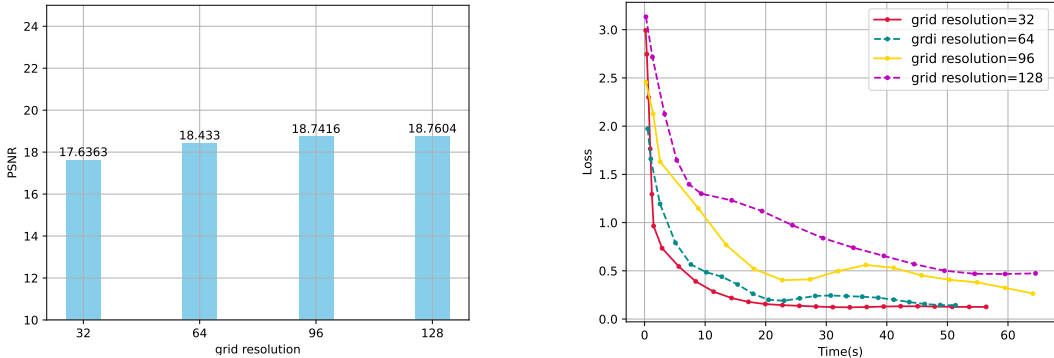


Figure 7: Convergence curves of the model with different training grid resolutions. PSNR metrics of the generated meshes surface are also compared.

### C.1 Training Grid Resolution

The resolution of the 3D density grid depicted in Figure 2 determines the computational complexity and details of mesh surface. In order to choose a suitable resolution for the grid, we conduct experiments using various resolutions, namely 32, 64, 96, and 128. As illustrated in Figure 7, we plot curves of loss under different settings throughout the training process. We also evaluate PSNR metrics of the images rendered from the final results. It can be seen that although the quality of reconstruction results enhances with increasing resolution, our model exhibits a slower convergence. Moreover, the convergence time at the resolution of 128 is significantly longer than the other three resolutions. However, compared with resolution of 96, where the model already has an acceptable performance, the improvements achieved at resolution of 128 are marginal. Therefore, we select 96 as our grid resolution is selected to strike a balance between generation speed and quality.

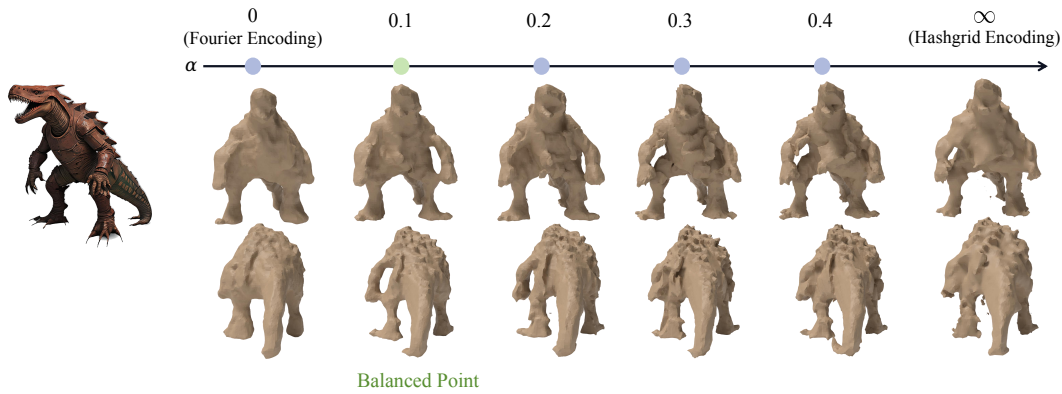


Figure 8: We study the effects of  $\alpha$  on our model. Increasing  $\alpha$  leads to a 3D geometry with more surface details but less precision. We find  $\alpha = 0.1$  provides a good balance.

## C.2 Choice of Combination Ratio $\alpha$

We conduct experiments with an increasing value of  $\alpha$  and compare their reconstruction geometry. We start from  $\alpha = 0$  to use only fourier encoding and gradually increase  $\alpha$  to 0.1, 0.2, 0.3, 0.4, and finally  $\infty$  to use only multi-resolution hash grid encoding. The comparison of results is illustrated in Figure 8. The key observations include: (1) Relying solely on fourier encoding generates over-smooth mesh surface with minimal details. (2) Relying solely on the hash grid encoding improves performance in recovering details, but generates a distorted shape. (3) As  $\alpha$  increases, the reconstructed geometry has more surface details but becomes more inaccurate. To strike a balance, we choose 0.1 for  $\alpha$ .

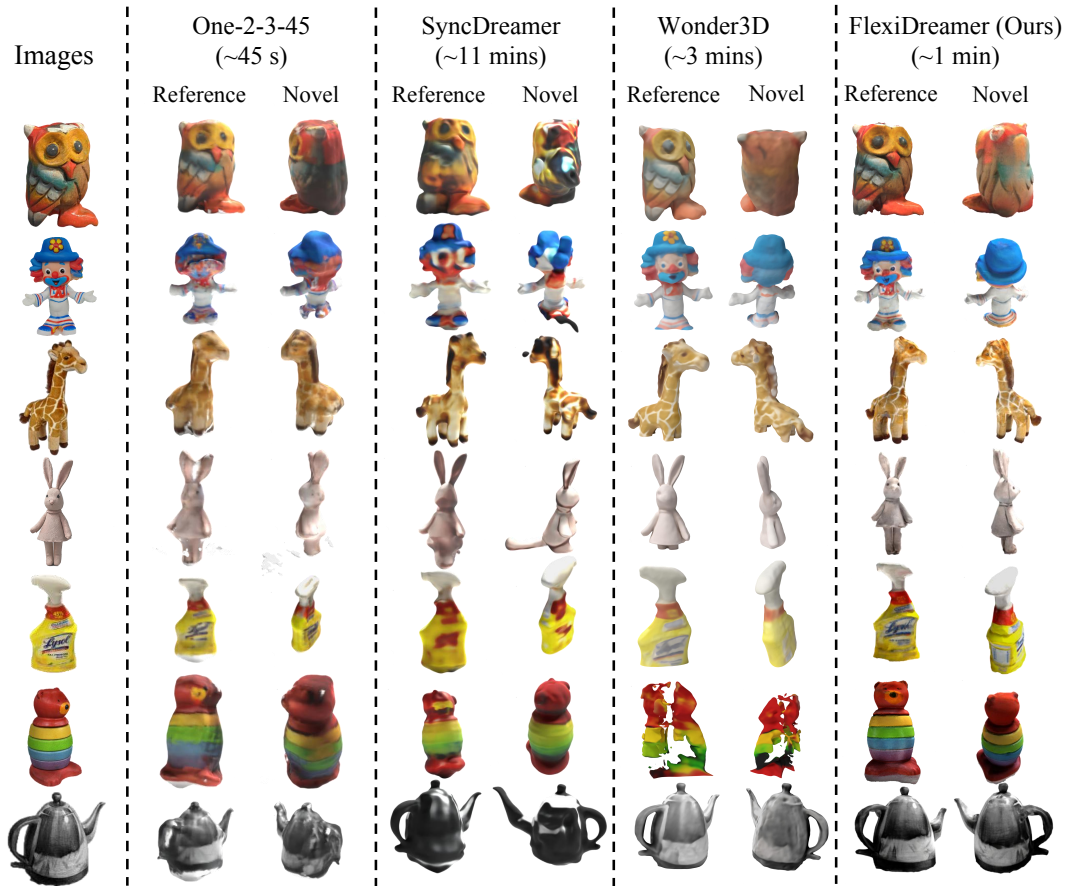


Figure 9: **Qualitative comparisons:** We compare FlexiDreamer with recent state-of-art single image-to-3D approaches.



## D More Comparisons and More Results

We additionally compare FlexiDreamer with baselines and show more visualization results respectively in Figure 9 and 10.



Figure 10: More generated results of FlexiDreamer.